polymers

MDPI

Article

Silicic Acid Polymerization and SiO_2 Nanoparticle Growth in Hydrothermal Solution

Vadim V. Potapov [1,*], Angel A. Cerdan [2] and Denis S. Gorev [1]

[1] Research Geotechnological Center, Far Eastern Branch of Russian Academy of Sciences, 30, Severo-Vostochny Highway, 683002 Petropavlovsk-Kamchatsky, Russia
[2] Chemical Department of Moscow State University, Leader Scientist, Russian Federation, Leninskie Gory, 1, 119991 Moscow, Russia
* Correspondence: vadim_p@inbox.ru

Abstract: The approach of numerical simulation of orthosilicic acid OSA polymerization and SiO_2 nanoparticle formation in hydrothermal solution have been developed based on the model of the homogeneous stage of nucleation and the subsequent growth of particles. The influence of surface tension on the interface of SiO_2–water, the rate of molecular deposition, and Zeldovich factor Z were evaluated. Temperature dependence on time, pH, initial OSA concentration, and ionic strength are the main parameters that determine the kinetics of colloid phase formation, the final average size of SiO_2 nanoparticles, and the particle size distribution and its polydispersity index. The results of the numerical simulation were verified with experimental data on OSA polymerization and measurement of nanoparticles sizes using the method of dynamic light scattering in a wide range of temperatures of 20–180 °C, pH = 3–9, SiO_2 content C_t of 300–1400 mg/kg, and ionic strength I_s of 0.0001–0.42 mol/kg. The results obtained can be used in the technology of hydrothermal synthesis of sols, gels, and nanopowders to regulate the kinetics of OSA polymerization and SiO_2 nanoparticle growth, particle size distribution, morphology, and structure of products.

Keywords: hydrothermal synthesis of SiO_2 nanoparticles; kinetics of orthosilicic acid polymerization; nanoparticle size distribution

Citation: Potapov, V.V.; Cerdan, A.A.; Gorev, D.S. Silicic Acid Polymerization and SiO_2 Nanoparticle Growth in Hydrothermal Solution. *Polymers* **2022**, *14*, 4044. https://doi.org/10.3390/polym14194044

Academic Editor: Il Kim

Received: 15 July 2022
Accepted: 19 September 2022
Published: 27 September 2022

1. Introduction

Hydrothermal synthesis of SiO_2 nanoparticles is the new technological method with a low production cost, high density of silanol groups, low toxicity, excluding the use of chemical reagents and other green chemistry methods of nanoparticle synthesis [1–3], and allows to obtain different forms of nanosilica—sols, gels, powders, products of the sol-gel process applied in concrete, agricultural plants, medicines, and other materials [4–7]. The technology of hydrothermal synthesis includes the stages of OSA polymerization, ultrafiltration membrane concentration of nanoparticles, the sol-gel process, vacuum sublimation, and others [4–6]. The temperature regime, the stage of polymerization, pH, initial OSA concentration C_s, and ionic strength influenced the rate of SiO_2 nanoparticle formation, the average nanoparticle size, and the index of polydispersity of nanoparticles in hydrothermal sols. Therefore, the density, morphology, agglomerate dimensions and fractal structures, volume, surface, diameters, and structure of pores of nanopowders produced from hydrothermal sols are also affected [4,5]. There is a need to regulate the parameters at the stage of OSA polymerization of silicic acid by means of numerical simulation to achieve the necessary characteristics of sols, gels, and nanopowders.

The kinetics of OSA polymerization with different mechanisms has been studied by many researchers under various conditions: pH, initial concentration of dissolved silica Cs, solution temperature, ionic strength, and sizes and molecular weight of SiO_2 particles formed.

At sufficiently high concentrations of silica in 2–6 wt.% sodium silicate salt solutions with the ratio SiO_2:Na_2O = 3.25 and with acidification at pH = 1.7, when the increase in molecular weight was accompanied mainly by the aggregation of small particles the degree of polymerization increased proportionally to the square root of the polymerization time [8].

At the monomer concentration of 0.24 % in the absence of salts [9,10], the average molecular weight at pH = 2.0 increased linearly depending on the square root of time; at pH = 3.2, 3.8, it increased proportionally with time; at pH = 4.36—linearly from the square of time. At pH = 2.2, temperature 90 °C, the average particle diameter was 1.3 nm. At a higher silica concentration of 8 g/L after about 150 h at pH = 3.0 or 75 h at pH = 2.0 the average molecular weight reached 300 SiO_2 with a smaller resulting particle size of 0.9 nm [11]. The average molecular weight of the newly formed polymerized acid prepared by removing Na from a solution of sodium silicate at pH= 2–3 was about 660 SiO_2 atoms [12]. At pH = 2.1, temperature 25 °C, in 0.24 wt.% SiO_2 solution after 60 days after the start of polymerization, the proportion of monomeric silica was 14% and the particle diameter was 1.4 nm [13]. At pH = 8.8, growth of particles occurred during 1 min, that is $3 \cdot 10^4$ times faster than at pH = 2.0. In studies performed at 25 °C, pH = 2.0, in the solution of monosilicic acid 2.4% SiO_2 for 24 days the particle diameter was 1.65 nm; after 8 days it was about 3.4 nm [14–16]. In a wide range of SiO_2 contents at pH =3.0 and pH = 6.1, the initial average diameter of the nuclei was 1.5 nm and the final particle size was about 3 nm [17]. In [18], after 30 days of polymerization at pH = 7.0 and 25 °C with a total concentration of SiO_2 in a solution of 0.4 g/L the diameter of nanoparticles corresponding to the solubility was 3.7 nm.

In the pH = 7.0–10.0 region, when colloid particles are formed, but the aggregation process cannot proceed, the reaction order was 3 [13,19]. However, in [20], at different initial concentrations of OSA the apparent "order" of the polymerization reaction was determined as equal to 2 at a pH above 2 and was equal to 3 at a pH below 2 [20], whereas the second-order reaction rate constant decreased.

It was found that the rate of polymerization was the greatest at pH = 8.3 and close to the maximum in the pH = 7.0–9.0 region, and at pH < 7.0 and pH > 9.0 it noticeably decreased [21].

The detailed study of polymerization in the wide area of concentrations of 0.2–1.8 g/L of silica and pH = 4.0–10.0 at 25 °C confirmed that there is an induction period during which the polymerization of the monomer is only slight or nonexistent. A decrease in the monomer content as it polymerizes at pH = 7.0 and 25 °C at an initial content of 0.05 wt. % occurred according to the law $0.37 \cdot (t - 0.35)^{-0.333}$ [22]. The induction period was 0.35 h. After 1 h after the decrease in the monomer content, silica particles began to grow rapidly without the formation of any intermediate product. The presence of a long induction period at pH = 4.5–5.5 and a temperature of 95 °C is shown in [23]. The induction period characterizes the metastability of the system and for aqueous silicic acid at pH = 7.75, t = 20 °C, C_s = 1450 mg/kg under mixing conditions it decreased from 3.25 to 2.75 h [20,21]. In the strongly acidic region, the rate of the process is proportional to $[H+]^{1.2}$ at pH < 1.8, and in the weakly acidic region at pH > 3.4 $-[OH-]^{0.9}$ [24,25]. The rate increases initially with an increase in temperature from 20 to 90 °C and decreases with a decrease in the initial OSA concentration [24,25]. The results obtained in [26] for OSA solutions with a SiO_2 content of 300–1200 mg/kg and low salinity in the temperature range from 5 to 180 °C confirmed that the temperature changes at a constant silica concentration do not significantly affect the increase in induction time at temperatures from 90 to 180 °C.

In a dimer–monomer mixture at pH = 2.0 [27] the polymerization mechanism and particle sizes differed from the results of monosilicic acid polymerization obtained for polycyclic polymer formation in [14–16]: at the beginning the discrete particles of less than 4 nm in size formed, then such particles aggregated [27].

Thus, the experimental data obtained by the authors showed significant differences in the values of the polymerization reaction order, the rate constant, the induction period, the sizes of the formed nanoparticles, and the different effects of temperature, pH, and ionic

strength on these parameters. Taking this into account, it is justified to use the method of numerical simulation of polymerization based on a certain mathematical model.

One of the mathematical models of orthosilicic acid polymerization is Fleming's model [28]. Fleming suggested that the process under study is characterized by two main areas of flow. In the first region, the initial concentration of silicic acid exceeds the pseudo-equilibrium concentration of Cx, and the polycondensation reaction is a first-order reaction both with respect to the difference (C_s-C_x) and with respect to the surface concentration of C_{SiO}-ionized groups of SiO^-, that is, the surface charge of colloid particles. The second area is defined by the condition $C_s < C_x$.

The decrease in the rate of transition of monomeric silica to colloid is explained using the Weres-Yi-Tsao model [29]. The authors studied two processes: the formation of colloid particles at the homogeneous stage of nucleation and the subsequent growth of particles due to OSA molecular deposition. From this model, developed on the basis of classical concepts of nucleation by Lose-Pound, it follows that the supersaturation of S_N (T), equal to C_s/C_e, C_e (solubility of amorphous silica in water at temperature T), and pH are the main factors determining the rate of nucleation I_N of silicic acid in an aqueous solution.

The authors of [30] used two methods to study the OSA polymerization, transfer in nanocolloids, and nanosilica precipitation in synthetic solutions based on the Na_2SiO_3 precursor: (1) the concentration model, when the rate of monomeric silica concentration C_s decrease is proportional to the 4-th order of $k_1 \cdot C_s^4$ and the rate of nanosilica transfer to precipitated silica is proportional to the 1-st order of $k_2 \cdot C_{nano}$; and (2) the supersaturated model, when the rate of monomeric silica concentration C_s decrease is proportional to the 4-th order of the difference $k_1 \cdot (C_s - C_e)^4$, C_e—solubility of amorphous silica in the water at 25 °C. In the wide range of initial C_s 240–1200 mg/kg, ionic strength 0.01–0.24 mol/kg, and pH = 3–7 it was obtained that constants k_1 and k_2 did not differ for concentration and supersaturation models. The models cannot predict the sizes and distribution of SiO_2 particles.

The method of molecular dynamic simulation for OSA polymerization was developed in [31,32] at the temperature up 2700 K and can provide the structure of polymerized clusters which was in accordance with the ^{29}Si NMR method.

The models with different orders of polymerization reaction [8], taking into account the concentration of OH^- groups [33] and ionic strength [28] have been used for analysis of experimental results of orthosilicic acid polymerization in hydrothermal solutions [34].

In [35], the model of Weres-Yi-Tsao [29] has been applied to experimental results in hydrothermal solutions because it can predict not only time dependence of the OSA concentration but also evaluate how the average size of SiO_2 nanoparticles depends on time. The main purpose of this work was to investigate nanoparticle size distribution dependence on the temperature, ionic strength, and other parameters of the polymerization process needed to regulate the characteristics of nanosilica sol, gel, and powders produced using the technology of hydrothermal synthesis [4–7]. For this purpose, it is necessary: (1) to study the dependence of surface tension σ_{sw}, rate of molecular deposition R_{md}, and Zeldovich factor Z on the temperature and pH to explain the mechanisms of their influence on the results of the polymerization process; (2) to examine the dependence of the average nanoparticle size and induction period on temperature, pH, and ionic strength; (3) to study the nanoparticle size distribution under conditions of time variable temperatures; (4) to verify the results of the numerical simulation with the experimental data in wide range of T, pH, and I_s; and (5) to compare the results of the numerical simulation under time-variable temperature conditions at different technological stages of the hydrothermal sol production with the results of determining the average size of SiO_2 nanoparticles and their size distribution using the DLS method.

2. Method of Numerical Simulation of OSA Polymerization

The initial concentration of molecules of orthosilicic acid formed due to dissolution of minerals of rocks [4–7] is determined using quartz solubility C_{cr} (mol/kg) of α-quartz in water at the temperature T(K) [36]:

$$\lg C_{cr} = -1.468 + \frac{252.9}{T} - \frac{3.217 \cdot 10^5}{T^2}. \quad (1)$$

After the hydrothermal solution reaches the surface pressure and the temperature decreases, the supersaturation of the solution depends on solubility C_e of amorphous silica [37]:

$$\lg C_e = -0.1185 - \frac{1.126 \cdot 10^3}{T} + \frac{2.3305 \cdot 10^5}{T^2} - \frac{3.6784 \cdot 10^7}{T^3}. \quad (2)$$

Polymerization of orthosilicic molecules in oversaturated solution is provided by the formation of siloxane bonds and dehydration:

$$H_4SiO_4 + H_4SiO_4 \rightarrow Si_2O_7H_6 + H_2O \quad (3)$$

The total silica concentration C_t in the solution is equal to the sum of the concentrations of colloid silica C_{col}, soluble silicic acid C_s, and ions of silicic acids C_{in}:

$$C_t = C_{col} + C_s + C_{in}. \quad (4)$$

The fraction of dimers does not exceed 1.0% from C_e, the fraction of trimers is no more than 0.1% [26], the fraction of tetramers and low-molecular cyclic polymers is less than 0.1%, and the fraction of C_{in} does not exceed 14.0%.

The physical and chemical characteristics of the hydrothermal solution from the Mutnovsky geothermal electric plant are presented in the Table 1.

Table 1. Characteristics of the hydrothermal solution from the Mutnovsky field, ionic strength I_s = 14.218 mmol/kg, $I_s = \sum c_j \cdot z_j^2/2$, c_j, z_j (concentration (mol/kg) and charge of the j-th ion in solution), ($z_{Na} = 1$, $z_K = 1$, $z_{Ca} = 2$, $z_{Mg} = 2$, $z_{Al} = 3$), pH = 9.35, elec trical conductivity σ_{el} = 1.1–1.3 mS/cm. nc—not calculated.

Component	Concentration	
	mg/L	mg equ/L
Na^+	239.4	10.413
K^+	42.0	1.074
Ca^{2+}	1.6	0.0798
Mg^{2+}	0.72	0.0592
$Fe^{2,3+}$	<0.1	<0.0053
Al^{3+}	0.27	0.033
NH_4^+	1.1	0.0609
Li^+	0.71	0.102
Total cation concentration	285.9	11.827
Cl^-	198.5	5.591
HCO_3^-	81.0	1.327
CO_3^{2-}	19.9	0.663
SO_4^{2-}	192.1	3.9995
HS^-	4.95	0.15
H_2S^0	5.92	-
F^-	n/d	n/d
Total anion concentration	496.5	11.73
H_3BO_3	106.9	nc
$(H_4SiO_4)_t$	1190	nc
$(H_4SiO_4)_s$	222	nc
Mineralization M_h	1638.9	nc

We developed the mathematical model [29] which is based on the calculation of the rate of nucleation I_N (nucl/(kg·s)) dependent on oversaturation S_N (T) = C_s/C_e:

$$I_N = Q_{LP} \cdot Z \cdot \left(R_{md} \cdot A_{cr} \cdot N_A \cdot \rho \cdot M_{Si}^{-1} \right) \cdot e^{-\frac{\Delta F_{cr}}{k_B \cdot T}}. \quad (5)$$

where ΔF_{cr} is the change in free energy due to the formation of a nucleus of critical radius R_{cr} with a surface area of $A_{cr} = 4 \cdot \pi \cdot R_{cr}^2$ and the number of SiO_2 molecules n_{cr}, σ_{sw} is the surface tension at the silica–water interface, R_{md} is the rate of molecular deposition of SiO_2 on a solid surface, kg/(m^2·s), $k_B = 1.38 \cdot 10^{-23}$ J/K, $M_{Si} = 0.060$ kg/mol, $N_A = 6.02 \cdot 10^{23}$ mol^{-1}, Q_{LP} is the Lothe–Pound factor, $Q_{LP} = 3.34 \cdot 10^{25}$ kg^{-1}, and Z is the Zeldovich factor, calculated as follows:

$$R_{cr} = 2 \cdot \sigma_{SW} \cdot \frac{M_{Si}}{\rho \cdot N_A \cdot k_B \cdot T \cdot \ln S_N}. \quad (6)$$

$$n_{cr} = \left(\frac{4\pi}{3} \right) \cdot \left(\frac{\rho \cdot N_A}{M_{Si}} \right) \cdot R_{cr}^3. \quad (7)$$

$$\Delta F_{cr} = \frac{\sigma_{SW} \cdot A_{cr}}{3} = \left(\frac{16 \cdot \pi}{3} \cdot \sigma_{sw}^3 \cdot \frac{M_{Si}}{\rho \cdot N_A \cdot k_B \cdot T \cdot \ln S_N} \right)^2. \quad (8)$$

$$Z = \left[-\left(\partial^2 \Delta F_{cr} / \partial n_{cr}^2 \right) / (2 \cdot \pi \cdot k_B \cdot T) \right]^{0.5} = \left(\frac{2}{3} \right) \cdot \left(\frac{3 \cdot M_{Si}}{4 \cdot \pi \cdot \rho \cdot N_A \cdot n_{cr}^2} \right)^{\frac{1}{3}} \cdot \left(\frac{\sigma_{sw}}{k_B \cdot T} \right)^{0.5}. \quad (9)$$

with $\rho = 2200$ kg/m^3—the density of amorphous silica.

The function R_{md}, which is the rate of molecular deposition of SiO_2 as a function of temperature and pH of the solution, is expressed as follows in the model [29]:

$$R_{md} = F\left(pH,\ pH_{nom}\right) \cdot k_{OH}(T) \cdot f_f(S_a) \cdot \left(1 - S_N^{-1}\right). \quad (10)$$

$$\lg k_{oH} = 3.11 - \frac{4296.6}{T}. \quad (11)$$

$$f_f = S_t^5,\ S_a < S_t. \quad (12)$$

$$f_f = S_t^5 + 5 \cdot S_t^4 \cdot (S_a - S_t),\ S_a > S_t. \quad (13)$$

$$\lg S_t = 0.0977 + \frac{75.84}{T}. \quad (14)$$

$$F\left(pH, pH_{nom}\right) = h_f \cdot f'(pH) + (1 - h_f) \cdot f'\left(pH_{nom}\right). \quad (15)$$

$$f'\left(pH_{nom}\right) = \frac{f\left(pH_{nom}\right)}{f(7.0)}. \quad (16)$$

$$\lg f = pH - pK_i + \lg\left[Na^+\right]. \quad (17)$$

The coefficient of surface tension σ_{sw} depends on temperature and pH via the function I(pH, pH_{nom}):

$$\sigma_{sw} = H_\sigma - T \cdot S_\sigma - 2.302 \cdot 10^{-3} \cdot n_0 \cdot k_B \cdot T \cdot I\left(pH, pH_{nom}\right). \quad (18)$$

$$I\left(pH,\ ph_{nom}\right) = 0.119 \int_{-\infty}^{pH} F\left(pH', pH_{nom}\left(pH'\right)\right) dpH'. \quad (19)$$

where $S_a = (1 - \alpha_i) \cdot S_N$, α_i is a fraction of silicic acid in ionic form, pH_{nom} = pH + lg([Na^+]/0.069), [Na^+] is an ion activity [Na^+], mol/kg, $pK_i = 6.4$, f(7.0) = 0.119, $h_f = 0.45$, H_σ and S_σ are specific enthalpy and entropy of silica surface in water, $H_\sigma = 63.68 \cdot 10^{-3}$ J/m^2, $S_\sigma = 0.049 \cdot 10^{-3}$ J/m^2·K, and $n_o = 6.84 \cdot 10^{18}$ m^{-2} [29].

Time dependence I_N (t) was calculated considering the induction time τ_{in} that is necessary to grow and form a stable population of the particles with sizes close to critical [29]:

$$I_N(t) = I_N \cdot \left(1 - e^{-\frac{Tp}{\tau_{in}}}\right). \quad (20)$$

$$\tau_{in} = 1.08 \cdot 10^{-6} \cdot (R_{md})^{-1} \cdot (Q_{LP} \cdot Z \cdot R_{cr}^2 \cdot e^{-\frac{\Delta Fcr}{k_B \cdot T}})^{-0.25}. \quad (21)$$

Initial values were entered: the temperature T, pH, concentration of ions and ionic strength of the solution, total silica C_t content, time step DT_p, initial radii R(I), and particle quantity MP(I) of every class "I". The Runge–Cutt method was used for the numerical simulation.

The total content of colloid, monomeric silica, and the current value of supersaturation were estimated:

$$M_{col} = \sum_{I=1}^{I=N} \frac{4 \cdot \pi \cdot \rho \cdot R^3(I) \cdot MP(I)}{3}. \quad (22)$$

$$C_s = C_t - M_{col}. \quad (23)$$

Solution degree of supersaturation S_N was:

$$S_N = \frac{C_s}{C_e(T)}. \quad (24)$$

Then, the calculation of values of σ_{sw}, R_{md}, R_{cr}, Z, τ_{in}, and $I_N(t)$ corresponding to the current values of S_N, pH, and T using the equations was undertaken.

The quantity of new particles appearing during the time DT_p in accordance with the current value of nucleation rate I_N on a given program step (N+1) was calculated and it was equal to the quantity of particles in the new class N+1:

$$MP(N+1) = I_N \cdot DT_p \quad (25)$$

The summary of the concentration of particles CONP was calculated in a program cycle:

$$CONP = \sum_{I=1}^{I=N+1} MP(I). \quad (26a)$$

The increment in mass DPM of every class "I" during the time DT_p was calculated:

$$DPM(I) = 4 \cdot \pi \cdot R^2(I) R_{md} \cdot DT_p \quad (26b)$$

The calculation of particle radius R(I) corresponding to a new value of particle mass in every class I was:

$$R(I) = (R^3(I) + \frac{3 \cdot DPM(I)}{4 \cdot \pi \cdot \rho})^{\frac{1}{3}}. \quad (27)$$

The mean values of R_a, R^2_a, and R^3_a in all classes of particles were estimated using the program cycle:

$$R_a = \sum_{I+1}^{I=N+1} \frac{R(I) \cdot MP(I)}{CONP}. \quad (28)$$

$$R_a^2 = \sum_{I+1}^{I=N+1} \frac{R^2(I) \cdot MP(I)}{CONP}. \quad (29)$$

$$R_a^3 = \sum_{I+1}^{I=N+1} \frac{R^3(I) \cdot MP(I)}{CONP}. \quad (30)$$

3. Results

3.1. Dependence of the Surface Tension σ_{sw}, Rate of Molecular Deposition R_{md}, and Zeldovich Factor Z on the Temperature and pH

The main factors influencing the rate of the nucleation process I_N and the final average particle size R_a are the degree of temperature T, the degree of supersaturation $S_N(t)$, and pH. In addition, the final result of the numerical simulation is influenced by the functions f(pH, pHnom) and i(pH, pHnom), specified in the Equations (10)–(19). The results of the calculation of the function f(pH) at different pH in the range from 4.0 to 8.7 are presented in Table 1.

With an increase in pH, the value of the f(pH) function increases (Table 2). Consequently, with an increase in pH, the rate of molecular deposition of R_{md} increases, and the R_{md} parameter will strengthen the tendency to decrease the final average particle size. With an increase in the initial concentration of C_s, the rate of molecular deposition also increases (Figures 1 and 2). An increase in temperature has an inhomogeneous effect on the rate of molecular deposition (Figures 1 and 2): first, due to the increase in the kinetics of the process with increasing temperature, the rate of molecular deposition increases, then R_{md} decreases, since with increasing temperature, the solubility of C_e increases, the supersaturation of S_N decreases, and the value of the rate of molecular deposition decreases. At a fixed pH, R_{md} reaches a maximum at a certain temperature and the value of this maximum increases with an increase in the initial concentration (Figure 2).

Table 2. Values of function f at different pH.

pH	f(pH)	pH	f(pH)	pH	f(pH)
4.0	0.00025	5.9	0.017	7.5	0.21
4.5	0.00079	6.0	0.022	8.0	0.32
5.0	0.0024	6.5	0.055	8.5	0.44
5.5	0.0075	7.0	0.119	8.7	0.49

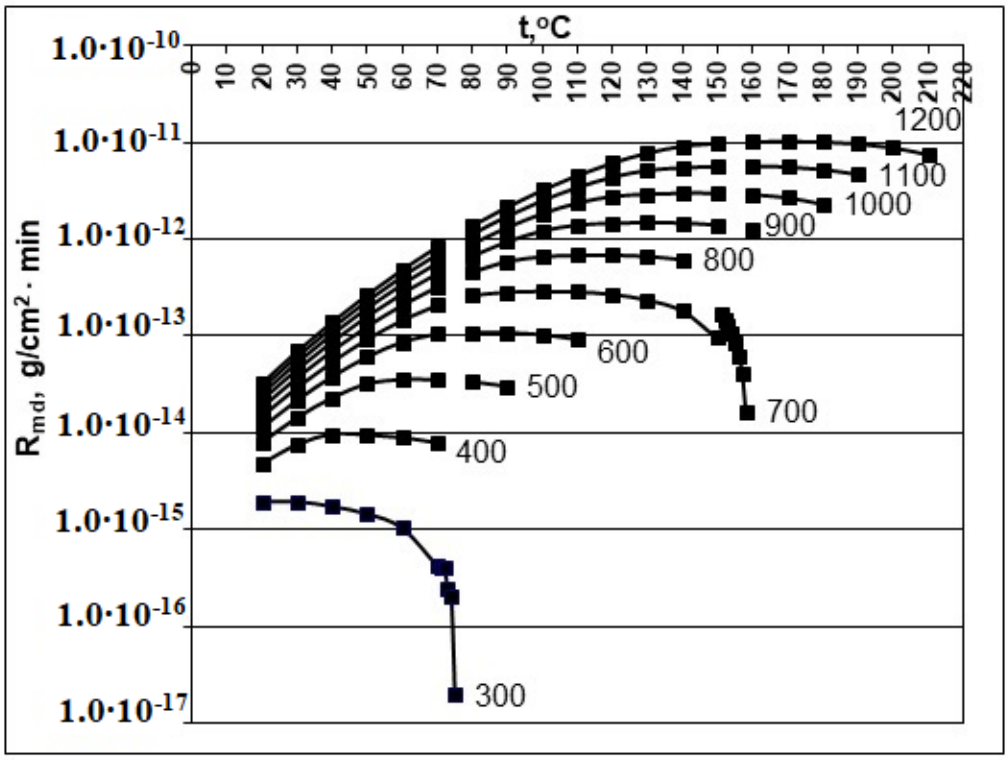

(**a**)

Figure 1. *Cont.*

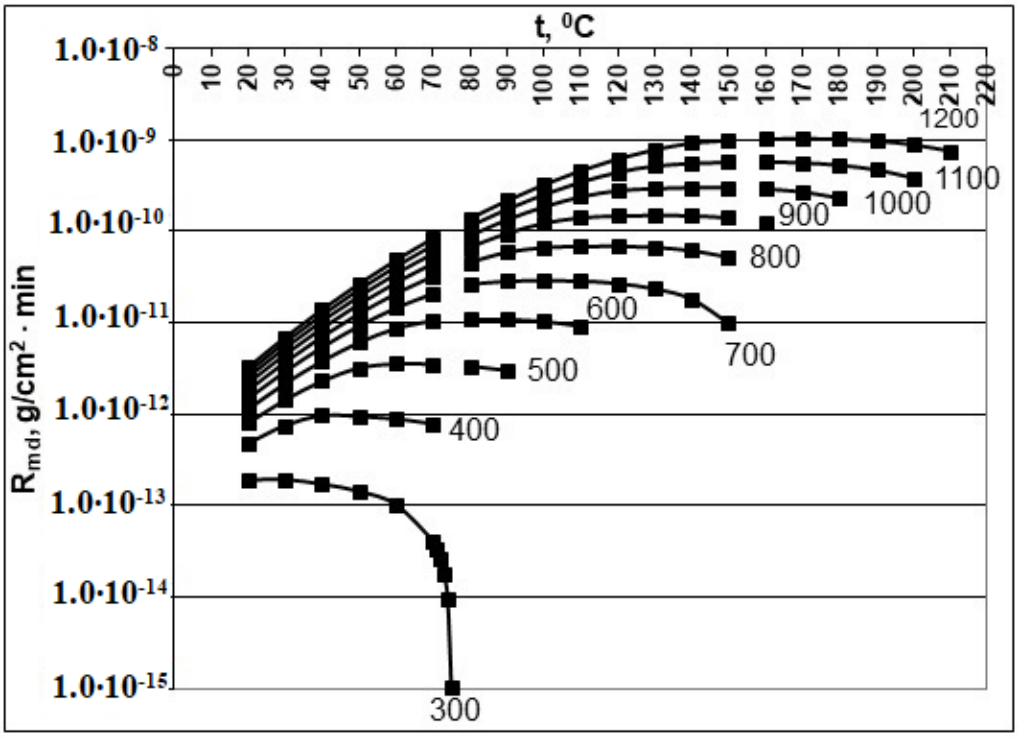

(**b**)

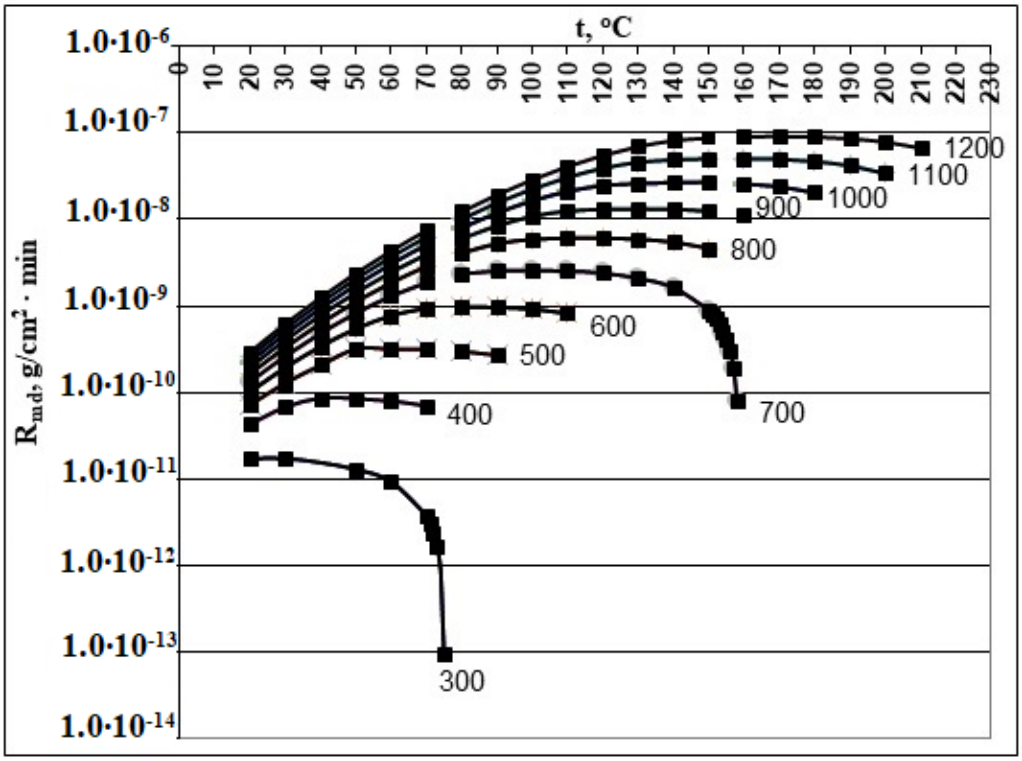

(**c**)

Figure 1. *Cont.*

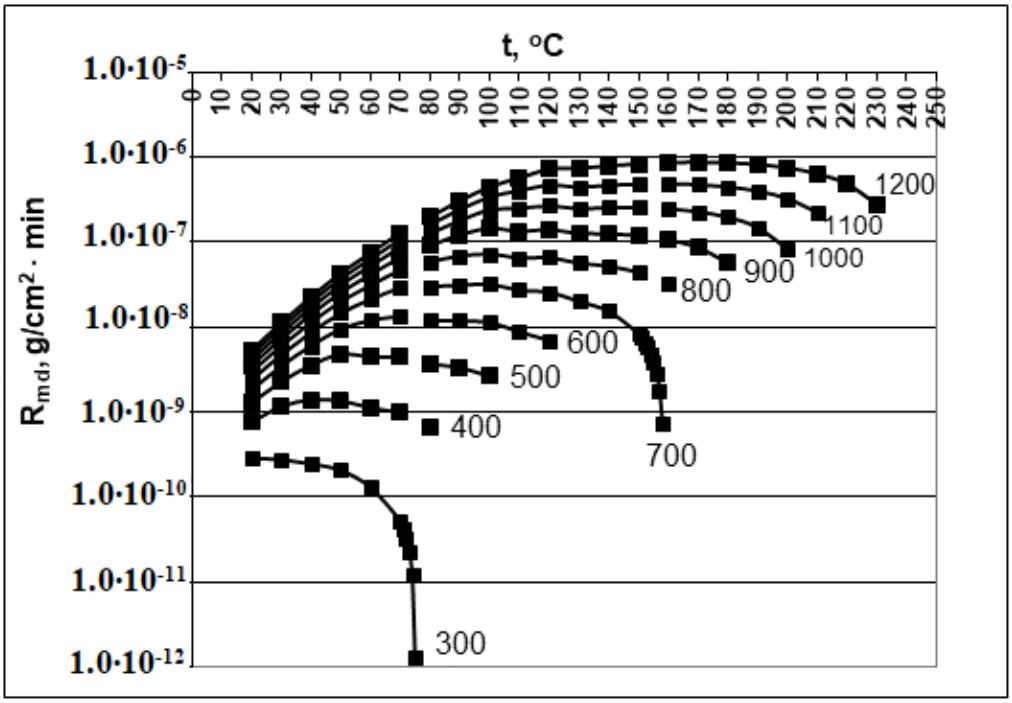

(**d**)

Figure 1. Dependence of the rate of molecular deposition R_{md} (g/(cm^2·min)) on the temperature t (°C) and concentration C_s (mg/kg). (**a**) pH = 2.0; (**b**) pH = 4.0; (**c**) pH = 6.0; (**d**) pH = 8.0. C_s = 300, 400, 500, 600, 700, 800, 900, 100, 110, and 1200 mg/kg.

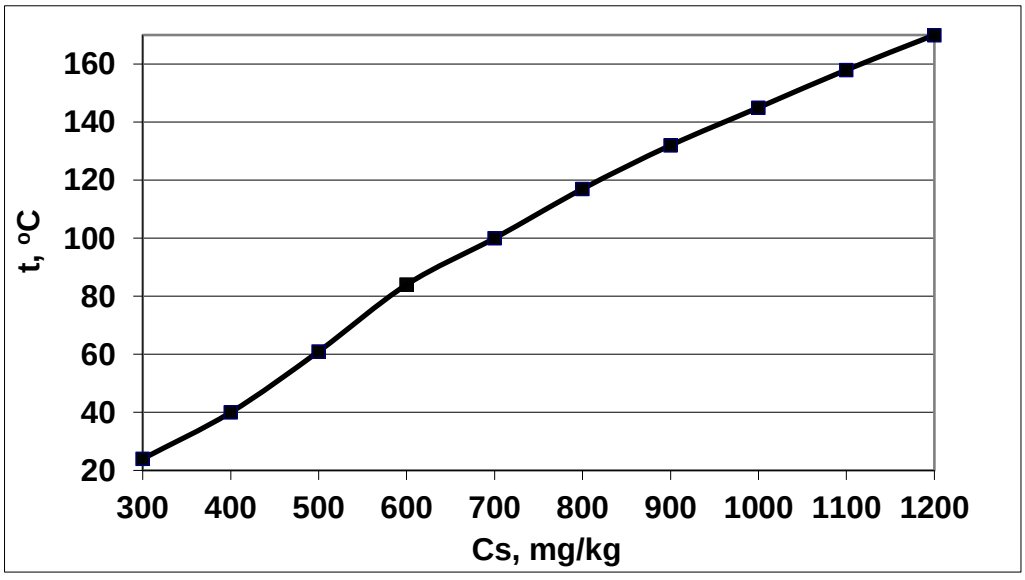

Figure 2. The temperature t (°C) corresponded to the maximum rate of molecular deposition R_{md} at different concentrations C_s, pH = 8.0.

An increase in the rate of molecular deposition with an increase in C_s and temperature will contribute to an increase in the rate of nucleation I_N of OSA and a decrease in the final average particle size.

The values of the function i (pH) in the range from 6.0 to 8.7 are presented in Table 3. With an increase in pH, the value of the function i (pH) increases. Consequently, the surface tension coefficient and the critical radius R_{cr} reduced. The surface tension coefficient σ_{sw} decreases with increasing temperature and with increasing pH in accordance with

Equations (18) and (19) (Figure 3a,b). Consequently, σ_{sw} will be a factor that, with an increase in temperature and pH, will contribute to a decrease in the critical radius R_{cr}, an increase in the nucleation rate I_N, and a decrease in the final average particle size R_a, competing with the factor of reducing supersaturation S_N.

Table 3. Values of function i at different pH.

pH	i (pH)
6.0	0.01
6.5	0.03
7.0	0.07
7.5	0.15
8.0	0.29
8.5	0.48
8.7	0.56

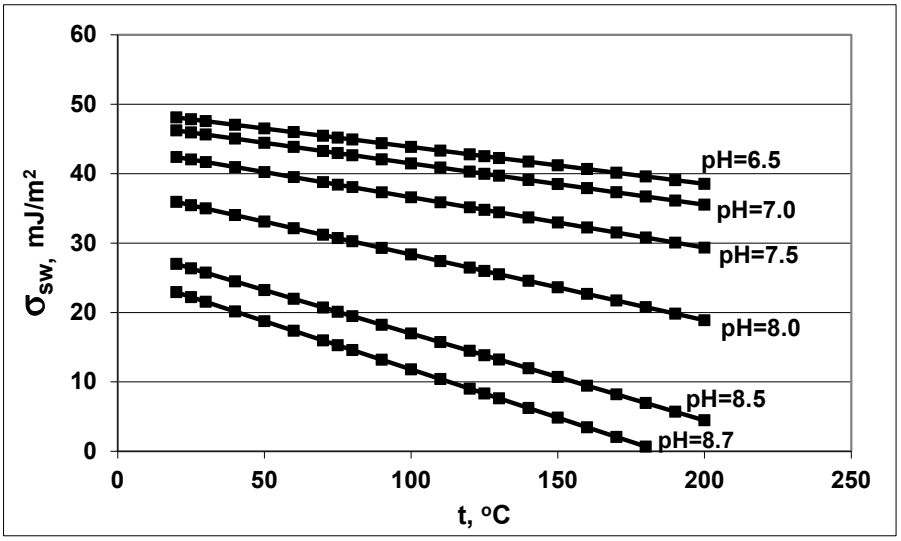

(**a**)

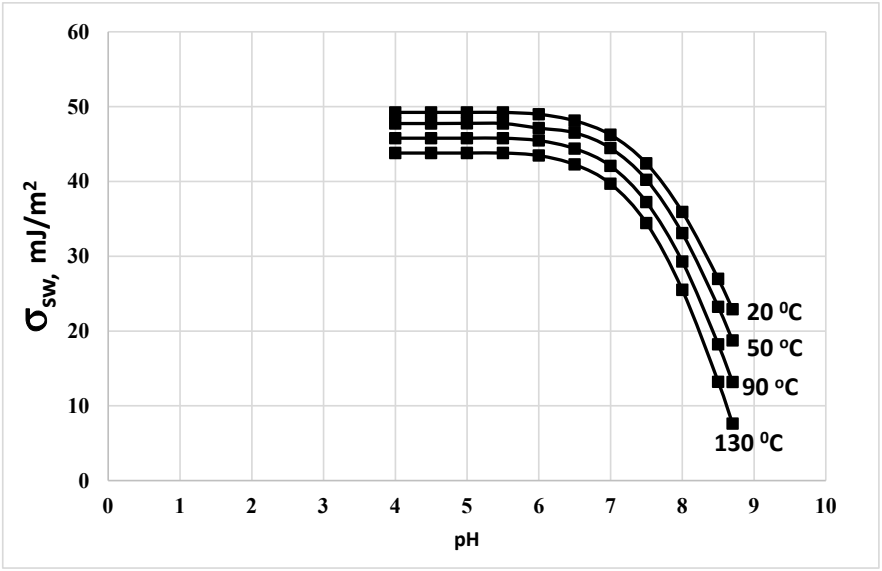

(**b**)

Figure 3. Dependence of the surface tension σ_{sw} (mJ/m^2) on (**a**) temperature t (°C) and (**b**) on pH. Initial concentration C_s = 700 mg/kg.

The physical meaning of the Zeldovich factor Z, calculated using Equation (9), is that only a certain proportion of particles whose sizes have reached a critical radius continue to grow further. The remaining particles decrease in size. At the same time, the concentration of particles whose sizes are higher than the critical radius is less than the equilibrium concentration. With an increase in temperature at a constant pH, the value of the Zeldovich factor decreases, and at the same time its effect on the rate of nucleation I_N competes with the opposite effect associated with a decrease in the supersaturation of S_N. An increase in pH leads to an increase in the values of the Zeldovich factor (Table 4).

Table 4. Dependence of Zeldovich factor Z on the temperature and pH (-).

t, °C	pH					
	4.0	**4.5**	**5.0**	**5.5**	**6.0**	**6.5**
20	$3.8 \cdot 10^{-2}$	$3.8 \cdot 10^{-2}$	$3.8 \cdot 10^{-2}$	$3.8 \cdot 10^{-2}$	$3.8 \cdot 10^{-2}$	$3.9 \cdot 10^{-2}$
50	$2.1 \cdot 10^{-2}$	$2.1 \cdot 10^{-2}$	$2.1 \cdot 10^{-2}$	$2.1 \cdot 10^{-2}$	$2.2 \cdot 10^{-2}$	$2.2 \cdot 10^{-2}$
100	$5.8 \cdot 10^{-3}$	-	$5.8 \cdot 10^{-3}$	$5.8 \cdot 10^{-3}$	$6.0 \cdot 10^{-3}$	$6.1 \cdot 10^{-3}$
130	$1.4 \cdot 10^{-3}$	$1.3 \cdot 10^{-3}$	$1.3 \cdot 10^{-3}$	$1.3 \cdot 10^{-3}$	$1.4 \cdot 10^{-3}$	$1.4 \cdot 10^{-3}$
t, °C	**pH**					
	7.0	**7.5**	**8.0**	**8.5**	**8.7**	**8.99**
20	$4.2 \cdot 10^{-2}$	$4.8 \cdot 10^{-2}$	$6.4 \cdot 10^{-2}$	$1.1 \cdot 10^{-1}$	$1.5 \cdot 10^{-1}$	$3.3 \cdot 10^{-1}$
50	$2.4 \cdot 10^{-2}$	$2.8 \cdot 10^{-2}$	$4 \cdot 10^{-2}$	$7.6 \cdot 10^{-2}$	$1.2 \cdot 10^{-1}$	$3.5 \cdot 10^{-1}$
100	$6.7 \cdot 10^{-3}$	$8.2 \cdot 10^{-3}$	$1.2 \cdot 10^{-2}$	$3.1 \cdot 10^{-2}$	$6.2 \cdot 10^{-2}$	$8.6 \cdot 10^{-3}$
130	$1.6 \cdot 10^{-3}$	$2 \cdot 10^{-3}$	$3.3 \cdot 10^{-3}$	$1 \cdot 10^{-2}$	$2.6 \cdot 10^{-4}$	-

3.2. Results of the Numerical Simulation at Different Temperatures and pH: Average Particle Size, Induction Period, and the Particle Size Distribution

The results of numerical simulation showed (Table 5) that when the temperature increases at a constant pH the final average size of SiO_2 nanoparticles increases because the degree of oversaturation and I_N become higher. When the pH decreases at a constant temperature the final average size increases (Table 5) due to the increase in the surface tension and the increase in the critical size of the nucleus R_{cr} and the decrease in I_N. If the initial concentration of orthosilicic acid increases the final average size decreases because the degree of oversaturation increases, I_N increases, and R_{cr} decreases (Table 6).

Table 5. The final average radius of silica particles at a constant temperature and varying pH (nm). $C_s(t = 0) = C_t = 700$ mg/kg.

pH	t, °C					
	20	**40**	**50**	**60**	**80**	**100**
4	5.28	19.24	48.06	156.55	6342.1	-
5	5.29	19.05	47.30	153.15	5858.7	-
6	2.98	16.82	40.69	128.01	4684.7	-
7	2.97	7.66	15.28	38.17	701.4	-
8	0.98	1.21	1.50	1.77	3.48	18.7
8.5	0.64	0.73	0.78	0.84	1.01	1.26

Table 6. Values of the final mean size of silica particles (nm) under different temperatures t and initial concentrations of solution C_s, pH = 8; (-) means that it was not estimated.

C_S, mg/kg	t, °C			
	20	**40**	**50**	**60**
300	93.5	-	-	-
350	12.4	1019.9	-	-

Table 6. *Cont.*

C_S, mg/kg	t, °C			
	20	**40**	**50**	**60**
400	4.35	49.1	586.3	-
500	1.79	4.08	8.96	32.7
600	1.246	1.84	-	3.80
700	0.98	1.21	-	1.77
800	0.87	1.05	-	1.31
1000	0.73	0.83	-	0.95
C_S, mg/kg	t, °C			
	70	**80**	**85**	**90**
300	-	-	-	-
350	-	-	-	-
400	-	-	-	-
500	-	-	-	-
600	7.56	24.14	56.14	169.8
700	-	3.48	-	6.49
800	-	1.81	-	2.30
1000	-	1.10	-	1.21

After nucleation and polymerization completion the fraction of dimers is not more than 1.0 % of solubility $C_e(T)$, the concentration of trimers is about 0.1 %, and the concentration of tetramers and polymers with circular structures of less than 6 units of SiO_2 is lower than 0.1 % [26].

The concentration of ions $H_3SiO_4^-$ and $H_2SiO_4^{2-}$ is not more than 14.0 % calculated from the dependences of constants of orthosilicic acid ionization of the first K_1 and second K_2 stages:

$$\lg K_1 = -\frac{2549}{T} - 15.36 \cdot 10^{-6} \cdot T^2 \quad (31)$$

$$\lg K_2 = 5.37 - \frac{3320}{T} - 20 \cdot 10^{-3} \cdot T \quad (32)$$

The function of oversaturation S_N vs. time T_p showed the long period of induction τ_{in} and homogeneous nucleation which becomes much longer at low values of pH when S_N changes slightly and the period of rapid growth of SiO_2 nanoparticles when S_N decreases sharply (Figures 4 and 5, Table 7). The number of new particles PNS depending on the duration of nucleation T_p reached a constant value when the rate of nucleation R_{nuc} rapidly decreased (Figures 4 and 5). The period of homogeneous nucleation increases when pH decreases and the initial degree of oversaturation S_N decreases at higher temperatures and low initial C_s concentrations (Table 7). The relation (t_{hom}/t_{hetg}) increases when the temperature increases and pH decreases (Table 7).

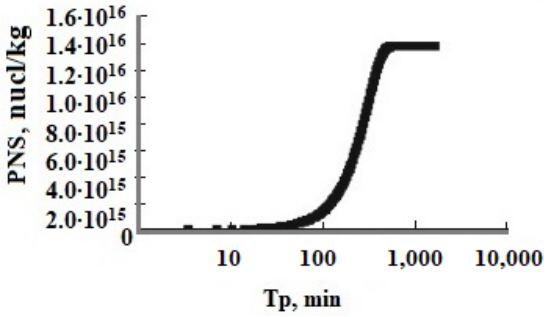

Figure 4. The number of new particles PNS (nucl/kg) versus time T_p; T = 50 °C, the initial concentration is C_s = 700 mg/kg, pH = 8.

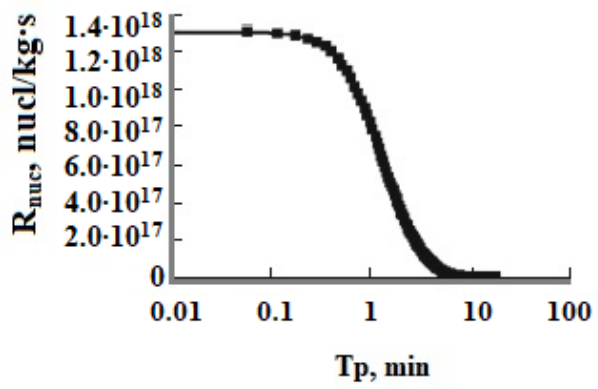

Figure 5. The rate of nucleation R_{nuc} (nucl/(kg·s)) versus time T_p; T = 50 °C, the initial concentration is C_s = 700 mg/kg, pH = 8.

Table 7. Durations of homogeneous t_{hom} and heterogeneous t_{hetg} nucleation at different temperatures, pH, C_s.

Temperature, °C	pH	Initial OSA Concentration C_s, mg/kg	t_{hom}. min	t_{hetg}, min	t_{hom}/t_{hetg}
20	5	700	80,385.3	4,369,195	0.018398
20	6	700	8255.45	454,617.5	0.018159
20	7	700	749.63	81,119.24	0.009241
20	8	700	50.20	5133.77	0.009779
50	5	700	118,281.1	3,027,579	0.039068
50	6	700	11,123.75	250,812.4	0.044351
50	7	700	715.87	20,328.97	0.035215
50	8	700	13.47	776.68	0.01735
80	5	700	4,352,938	$7.15 \cdot 10^7$	0.0608
80	6	700	373,867.6	5,574,710	0.067065
80	7	700	10,519.41	143,413.7	0.07335
80	8	700	19.635	328.12	0.05984
100	5	700	$7.07 \cdot 10^9$	$5.32 \cdot 10^{10}$	0.133
100	6	700	$4.89 \cdot 10^8$	$3.53 \cdot 10^9$	0.139
100	7	700	32,828.60	$2.19 \cdot 10^7$	0.15
100	8	700	116.61	638.40	0.182
120	5	700	$1.08 \cdot 10^{19}$	$4.94 \cdot 10^{19}$	0.219
120	6	700	$3.93 \cdot 10^{17}$	$1.78 \cdot 10^{18}$	0.22
120	7	700	$4.71 \cdot 10^{13}$	$1.87 \cdot 10^{14}$	0.252
120	8	700	26,324.92	73,435.34	0.3584

In Figure 6, the distributions of the number of particles vs. radius formed at constant T = 50–60 °C, pH = 4 and 8, and initial OSA concentrations C_s = 700 and 800 mg/kg are shown. The form of the function of SiO_2 particle number distribution by radius has a maximum corresponding to the average radius R_a. Figure 6 shows an asymmetrical distribution, that is the right branch of the silica particle size distribution formed at constant temperature is convex and the left branch is concave.

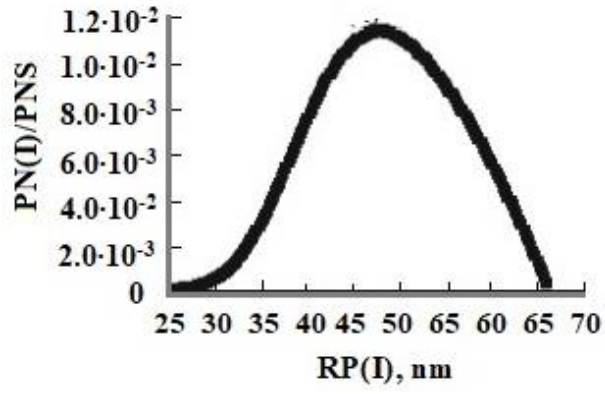

(**a**)

Figure 6. *Cont.*

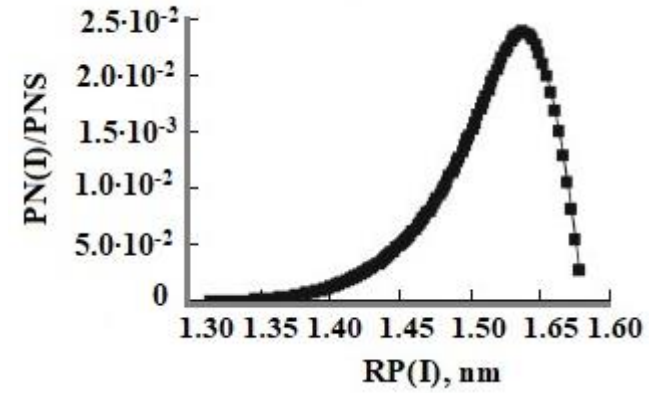

(**b**)

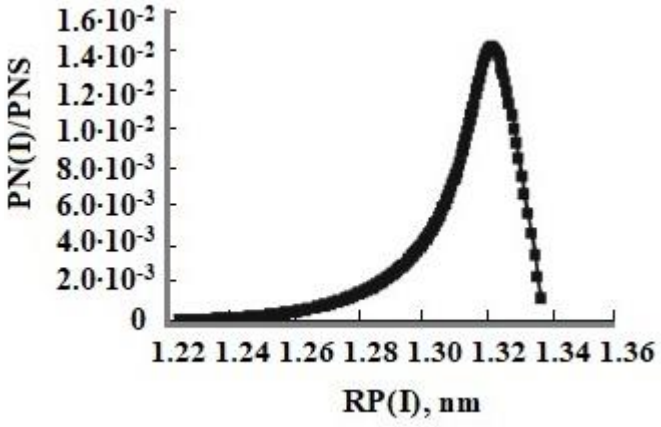

(**c**)

Figure 6. The particle size distribution at different pH and initial OSA concentrations C_s. (**a**) T = 50 °C, C_s = 700 mg/kg, pH = 4; (**b**) T = 50 °C, C_s = 700 mg/kg, pH = 8; (**c**) T = 60 °C, C_s = 800 mg/kg, pH = 8. PNS—total quantity of the formed SiO_2 particles.

The average radius of SiO_2 nanoparticles and the distribution by radius were determined using the method of dynamic light scattering (DLS). Values R_a were in the range from 5.0 up to 20.0 nm and values of particles radii were in the range from 1.0 up to 50.0 nm [4–7].

3.3. Simulation of OSA Polymerization at Different Ionic Strengths

The dependence of C_s (T_p) is also affected by the ionic strength of the I_s solution. The simulation results were obtained at t = 20 °C, pH = 8.0, and C_s = 700 mg/kg and various values of I_s: 0.014, 0.07, 0.14, 0.28, 0.4, 0.8, 1.0, 1.2, 1.4, 7.1, 10.6, and 14.2 mol/kg. With an increase in I_s from 0.014 to 0.8 mol/kg, the $C_s(T_p)$ dependence shifts to the left and acquires a concave shape (Figure 7a,b). In the range of ionic strength values from 0.8 to 1.4 mol/kg, with an increase in I_s, the rate of decrease of C_s(Tp) was lower and the curves shift to the right. The shape of the curves becomes convex. At values of I_s > 1.4 mol/kg, the curves C_s (T_p) are shifted to the left again.

The dependence of the final average particle size on the ionic strength of the I_s solution is non-monotonic also (Table 8, Figure 8). With an increase in I_s from 0.014 to 0.8 mol/kg, R_a increases. Starting from the value I_s = 0.8 mol/kg, the final average particle size decreases. This non-monotonic dependence is explained by the fact that with an increase in I_s, the rate of molecular deposition of R_{md} increases due to an increase in the degree of ionization of orthosilicic acid α_{SIL}. Therefore, the rate of nucleation of OSA I_N increases (Equation (5)). At the same time, the growth rate of the formed particles increases (Equation (10)). Thus, the final average size of silica particles is influenced by

two competing factors—growth of I_N and R_{md} which determines the non-monotonic behavior of the R_a (I_s) dependence.

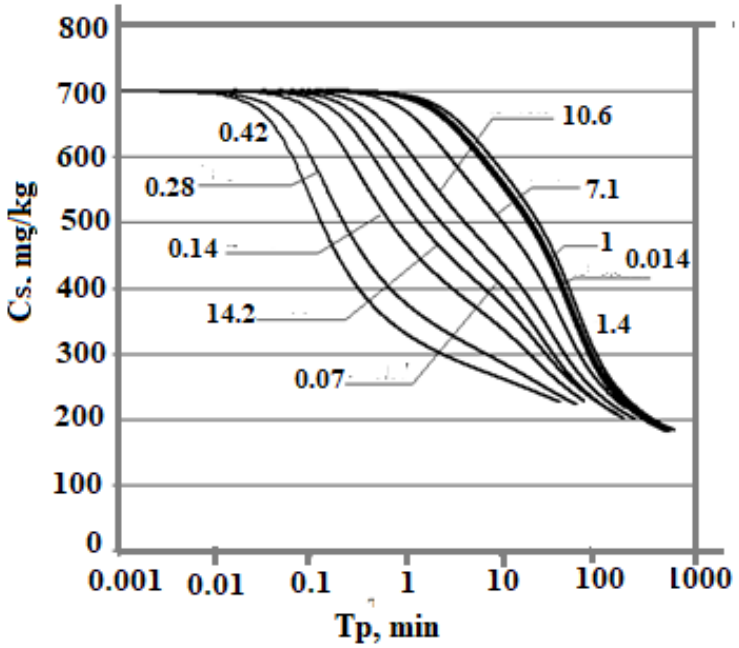

(**a**)

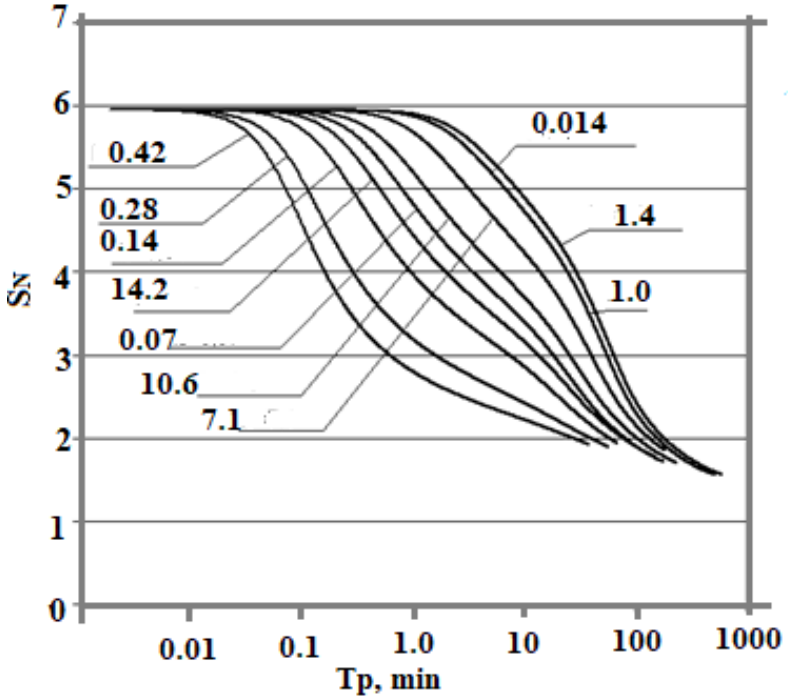

(**b**)

Figure 7. The dependence of the concentration of dissolved silicic acid (**a**) and supersaturation (**b**) on time. t = 20 °C, pH = 8.0, initial concentration C_s = 700 mg/kg, and various values of ionic strength (mol/kg).

Table 8. The final average size of silica particles in solutions with different ionic strength values. t = 20 °C, pH = 8.0, and C_s = 700 mg/kg.

I_S, mol/kg	R_a, nm	I_S, mol/kg	R_a, nm	I_S, mol/kg	R_a, nm
0.014	0.99	0.4	1.048	1.4	1.042
0.07	1.029	0.8	1.049	7.1	0.9
0.14	1.036	1.0	1.047	10.6	0.79
0.28	1.044	102	1.045	14.2	0.7

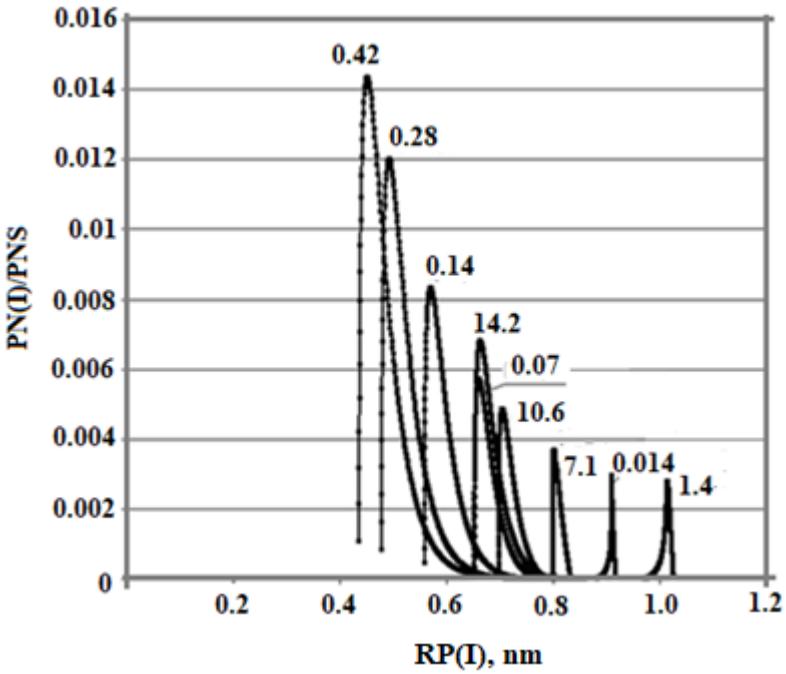

Figure 8. Particle size distribution with different ionic strength values. t = 20 °C, pH = 8.0, and initial concentration C_s = 700 mg/kg, I_s (mol/kg).

3.4. Simulation of OSA Polymerization under Time-Variable Temperatures

A significant influence of the variable temperature regime on the rate of the OSA nucleation process and the final average size of silica particles was revealed.

To simulate the process of nucleation of OSA under variable temperature conditions, the following law of temperature t reduction with polymerization time T_p was chosen:

$$t = t_2 + (t_1 - t_2) \cdot e^{\frac{-T_p}{taun0}} \quad (33)$$

Dependence (1.34) corresponds to the rate of heat q, W/(m^2·s) exchange with an environment with a constant temperature t_o according to Newton's law $q = \alpha \cdot F \cdot (t - t_0)$, t_1, t_2 are the initial and final temperatures of the solution; α—coefficient of heat exchange W/(m^2·s·°C); F—area of heat exchange, m^2; taun0—the characteristic cooling time of the solution. Calculations were performed at t_1 = 100 °C and t_2 = 20 °C for solutions of the Mutnovsky hydrothermal field at C_s = 700 mg/kg and pH = 8.0; taun0 was taken to be 120, 240, 360, and 480 min.

Figure 9 shows that the smaller the tun0, the higher the level of supersaturation of S_N. Consequently, the rate of OSA nucleation increases. This leads to a decrease in the final average particle size.

The effect of the initial concentration on the rate of the nucleation process and the final average size of silica particles in the variable temperature regime turned out to be ambiguous. The temperature was lowered from 100 to 20 °C, pH = 8.0, and taun0 = 360 min. The

initial concentration assumed various constant values—500, 600, 700, 800, and 1000 mg/kg. Figure 10 shows a comparison of the dependencies obtained.

At variable temperatures, the supersaturation functions of time have a non-uniform behavior. The supersaturation of the solution $S_N = C_s/C_e$ depends on the solubility of C_e, which decreases, and faster than the value of the concentration of C_s.

Figures 9c and 10c show a more symmetrical distribution, that is both branches of the silica particle size distribution are convex in contrast to the case of constant temperatures when the right was convex and the left was concave. Thus, the temperature regime at the stage of polymerization strongly influenced the index of polydispersity of hydrothermal sols and the density, morphology, agglomerate dimensions, volume, surface, diameters, and structures of pores of nanopowders produced from hydrothermal sols [5].

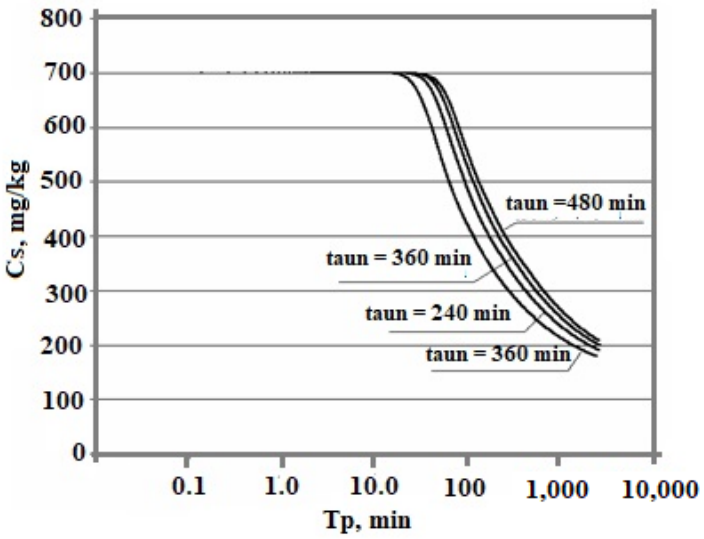

(**a**)

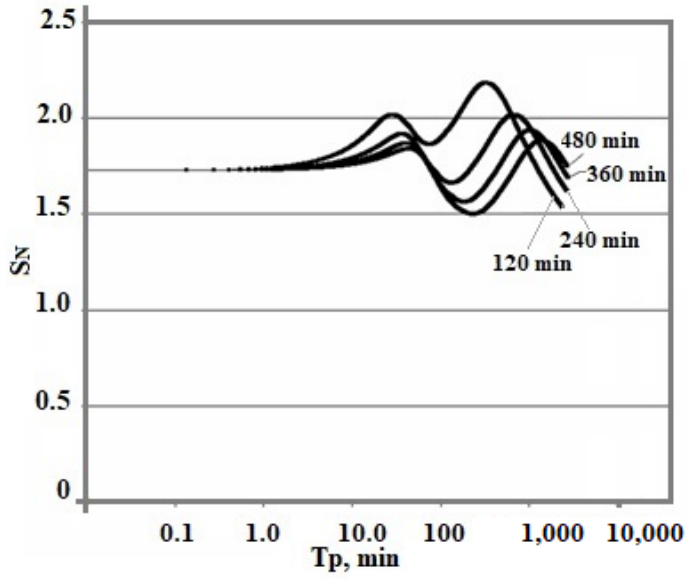

(**b**)

Figure 9. *Cont.*

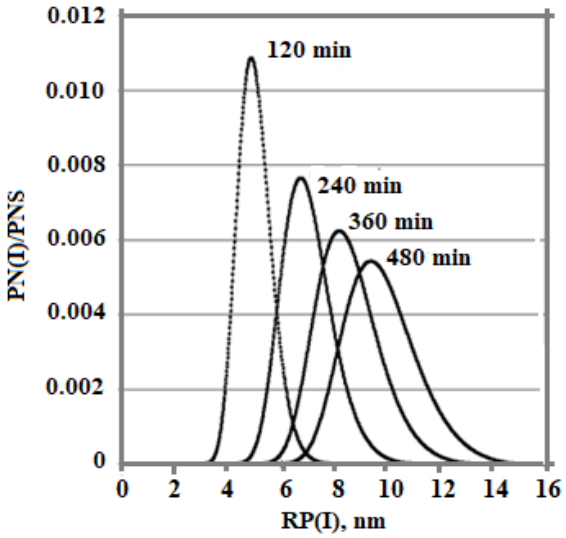

(**c**)

Figure 9. The time dependences of the concentration of dissolved silicic acid C_s (**a**), supersaturation (**b**), and particle size distribution (**c**). The temperature decreases from 100 to 20 °C, pH = 8.0, and C_s = 700 mg/kg.

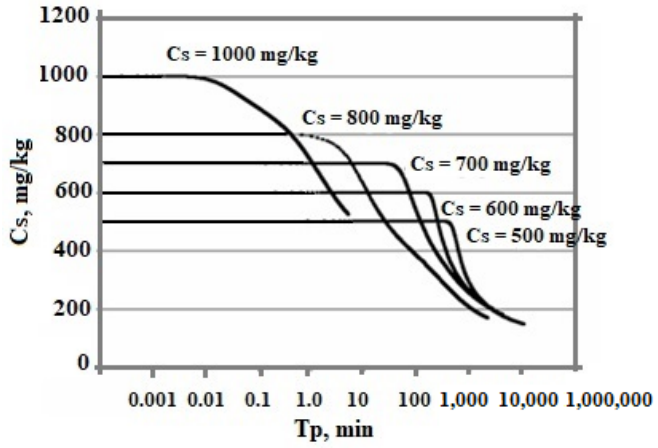

(**a**)

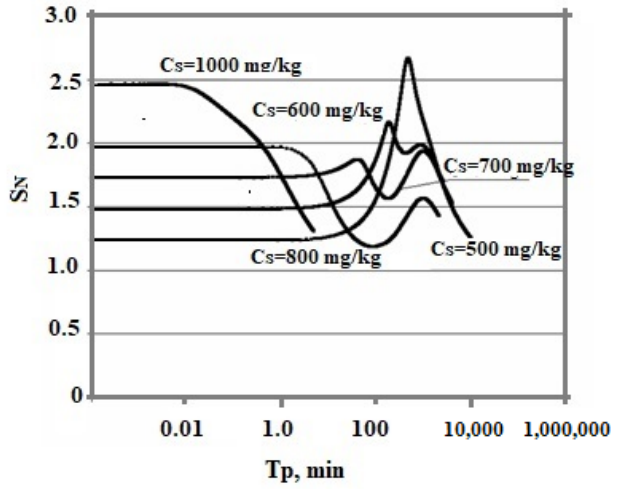

(**b**)

Figure 10. *Cont.*

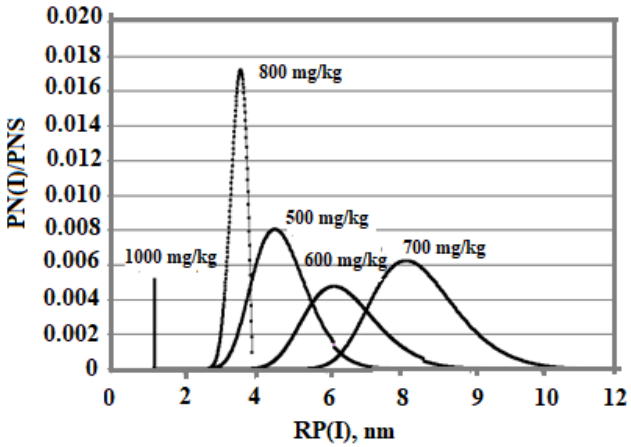

(**c**)

Figure 10. Dependence of C_s on T_p (**a**), S_N on T_p (**b**), and particle size distribution (**c**). The temperature decreases from 100 to 20 °C and taun0 = 360 min.

3.5. Comparison of the Experimental Data with Results of the Numerical Simulation

Experimental data $C_s(T_p)$ obtained in sodium silicate solutions with Na^+ cations removed by ion exchange and low ionic strength [26] were in agreement with the results of numerical simulation in the wide range of temperatures and initial OSA concentration C_s (Figure 11) [35]: t = 30, 90, 120,150, 180 °C, C_s = 383, 620, 110, 1200 mg/kg, pH = 7.0, 7.4, 7.85; I_s = 0.000132–0.00134 mol/kg.

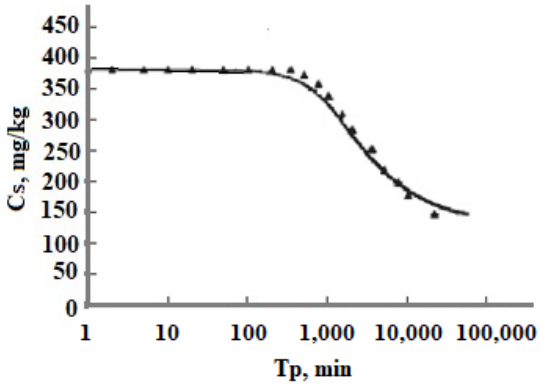

(**a**)

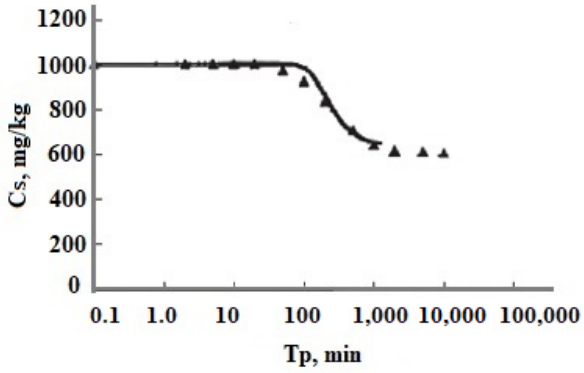

(**b**)

Figure 11. Comparing the experimental data [19] with the results of the numerical simulation. (**a**) t = 30 °C, C_s = 383 mg/kg, pH 7.0; (**b**) t = 150 °C, C_s = 1008 mg/kg, pH 7.85. I_s = 0.000132–0.00134 mol/kg. ▬—results of the simulation; ▲—experimental data.

The comparison of the experimental data on OSA polymerization and the results of the numerical simulation for the solution of the Pauzhetsky hydrothermal field showed that the discrepancy of about 12–14.2% was within the uncertainty of the yellow molybdate method for determining the concentration of dissolved silicic acid for the following conditions [35]: t = 20 °C; C_s = 315.6–338 mg/kg; pH = 8.2–8.35; and I_s = 0.04284 mol/kg.

The results of the simulation of OSA polymerization at the temperatures of 84–95 °C and high ionic strength for solutions with different chemical compositions showed an agreement with the experimental data obtained at Wairakei and Broadlands hydrothermal fields [35]: t = 84 °C, pH = 8.1, and C_s = 570 mg/kg (Wairakei); t = 95 °C, pH = 8.0, and C_s = 620 mg/kg (well 11 at Broadlands); t = 95 °C, pH = 7.7, and C_s = 900 mg/kg (well 22 at Broadlands); I_s = 0.05–0.06 mol/kg.

The results of the simulation of the distribution of the number of SiO_2 nanoparticles vs. radius for solutions in which OSA polymerized at the temperatures 33–43 °C, pH = 6.7–8.1, C_s = 366–546 mg/kg, and I_s = 0.043 mol/kg corresponded to the results of particles radii measured using the DLS method [35,38] in the range of 50–225 nm.

The experimental results of [24,25] on the maximum nucleation rate v_{max} determined as $(C_{s1} - C_{s2})/(T_{p2} - T_{p1})$ were in agreement with the results of the numerical simulation in the region of pH = 4–6, in which the model used [35] was applicable (pH = 4–8).

The comparison of the average diameter measured using helium chromatography in a synthetic solution with an initial C_s = 880 mg/kg at 20 °C and pH = 7.0 [39] were in good agreement with results of the numerical simulation [35].

The values of the k_1 constant for concentration and supersaturation models obtained in [30] for synthetic solutions in the wide range of initial C_s 240–1200 mg/kg, ionic strength 0.01–0.24 mol/kg, and pH = 3–7 corresponded to the times T_p of C_s decrease calculated in our numerical simulations for the same conditions.

The experimental results [35] with $C_s(T_p)$ curves characterized by k_p constants of the OSA reaction of the polymerization at different temperatures 20–50 °C, different pH = 4–8.5, and ionic strengths 0.01–1.1 mol/kg corresponded to the models [8,28,33].

4. Simulation the Particle Size Distribution in Hydrothermal Sol Production Technology

The technological flow sheet for the solution of the Mutnovsky geothermal electric power plant GeoPP includes the well, separator, pipe silencer, tank for the solution cooling and aging to develop OSA polymerization, ultrafiltration membrane module, and volumes for concentrated sol, Figure 12a. The temperature decreases with the linear dependence in every element from the well to silencer from 300 to 96 °C at pH = 8.0 and with the dependence (1.33) in the aging tank in which the temperature decreases from 96 to 70 °C. When the duration of aging was 20 h and taun = 11 h, the average SiO_2 nanoparticle radius calculated using the numerical simulation was 12.5 nm (Figure 12b) and it was 12.9 nm measured using the DLS method (Figure 13). When the duration of aging was 100 h and taun = 15 h, the final average diameters were 68.6 and 66 nm using the DLS method. If pH = 5.0, the temperature decrease during aging of 24 h was from 96 to 23 °C, taun = 12 h, and the calculated diameter was 160 nm and the diameter measured using the DLS method was 154 nm.

The temperature and aging duration can be varied to regulate the average particle diameter from 5 to 160 nm.

For the solution from wells at Cerro Prieto GeoPP with the values C_s = 950 mg/kg, pH = 7.3, I_s = 0.4227 mol/kg, aging duration 65 min, taun = 60 min, and temperature decrease from 100 to 30 °C [23,24], the final average radius calculated in the present work was R_A = 1.32 nm and it was 1.35 nm as a result of the calculation in [29].

For the solutions of the Wairakei GeoPP, New Zealand, at aging temperatures of 70 and 20 °C during 50 h, C_s = 490 mg/kg, and I_s = 0.05 mol/kg, the calculated average radii were 60.7 and 9.5 nm, and the radii measured using DLS were 60 and 10 nm.

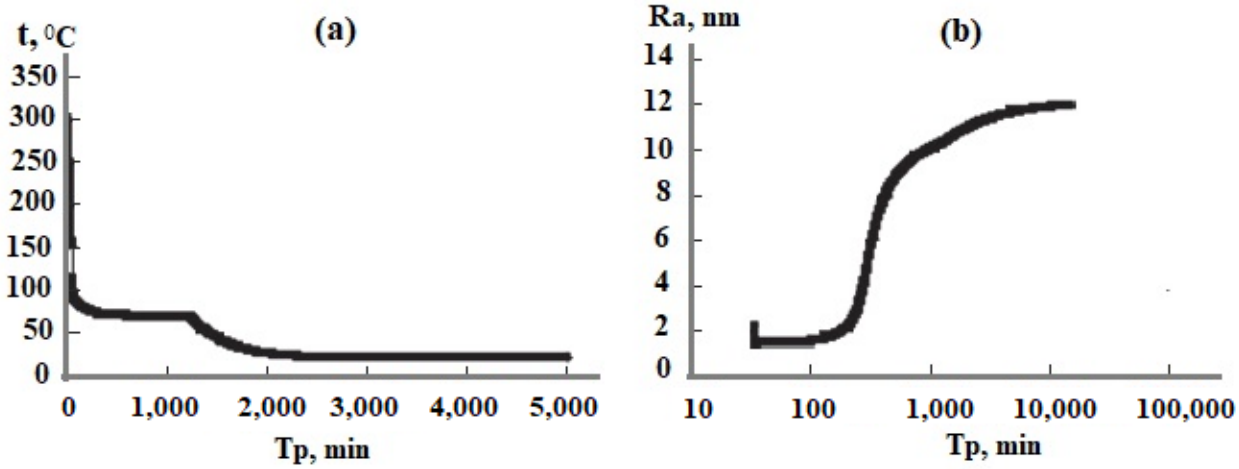

Figure 12. Parameters involved in the technological flow sheet of silica extraction. (**a**) Temperature versus time; (**b**) average silica particle radius as a function of time.

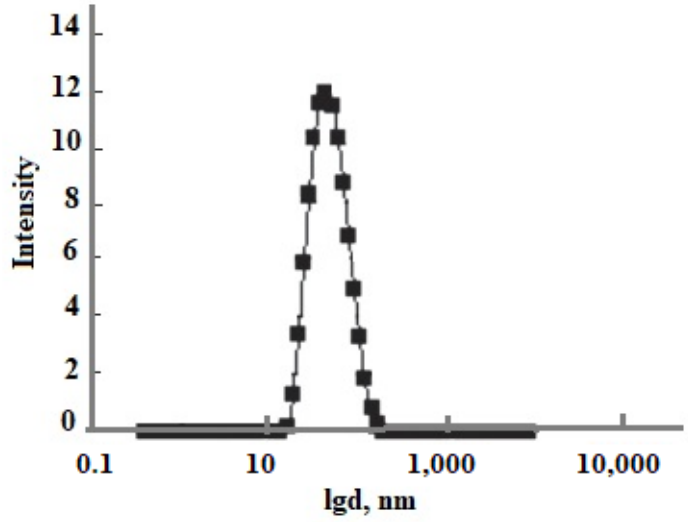

Figure 13. The particle size distribution based on DLS results. d is the particle diameter, nm. Well 054 at the Mutnovsky field.

5. Conclusions

The mathematical model we adopted allowed us to investigate the influence of various physical and chemical factors in a wide range of values on the rate of polymerization of OSA in a hydrothermal solution and on the SiO_2 nanoparticle size distribution. The results of the numerical simulation were verified using a comparison with experimental data. The temperature, pH, initial OSA concentration, and ionic strength are the main parameters that determine the kinetics of colloid phase formation, the final average size of SiO_2 nanoparticles, and the form of the particle size distribution.

The final average radius decreases when the temperature decreases, and the degree of oversaturation becomes higher taking into account the surface tension, rate of molecular deposition, and Z-factor. The average radius increases when the pH decreases due to the increase in the surface tension and the critical size of the nucleus. The average radius decreases when the initial OSA concentration and degree of oversaturation increases.

The function of oversaturation S_N depending on the time of polymerization T_p showed the long period of induction τ_{in} and homogeneous nucleation which becomes much longer at low values of pH. The period of homogeneous nucleation increases when pH decreases and the initial degree of oversaturation S_N decreases at higher temperatures and low initial

C_s concentrations. The relation of homogeneous and heterogenous durations (t_{hom}/t_{hetg}) increases when the temperature increases and pH decreases.

The dependence of the curve C_s vs. T_p and final average particle size R_a on the ionic strength I_s is non-monotonic. With an increase in I_s from 0.014 to 0.8 mol/kg, the kinetics of OSA polymerization accelerate, but R_a increases. Starting from the value of I_s = 0.8 mol/kg, the final average particle size decreases. This non-monotonic dependence is explained by the fact that with an increase in I_s, the rate of molecular deposition of R_{md} increases due to an increase in the degree of ionization of orthosilicic acid α_{SIL}. Therefore, the rate I_N of OSA nucleation increases. At the same time, the growth rate of the formed particles increases. Thus, the final average size of silica particles is influenced by two competing factors—the increases in I_N and R_{md} which determine the non-monotonic behavior.

At variable temperatures, the supersaturation functions of time have a non-uniform behavior. The supersaturation of the solution $S_N = C_s/C_e$ depends on the solubility of C_e, which decreases, and faster than the value of the concentration of C_s. Both branches of the silica particle size distribution are concave in contrast to the case of constant temperatures. The variation in temperatures during the stage of OSA polymerization can influence the index of polydispersity of particles, its distribution regarding sizes, and the homogeneity and symmetrical form of the distribution. The temperature regime at the stage of polymerization highly influenced the index of polydispersity of hydrothermal sols and, thus, the density, morphology, agglomerate dimensions and fractal structures, volume, surface, diameters, and structures of pores of nanopowders produced from hydrothermal sols.

The results obtained can be used for regulating the kinetics of SiO_2 nanoparticle formations, sizes, the polydispersity of the distribution of sizes, and the concentrations of nanoparticles in the technology of the hydrothermal synthesis of sol, gel, and powder.

The results can be applied to the technology of the production of synthetic water sols based on Na_2SiO_3 precursors and the technology of precipitated silica.

Author Contributions: Conceptualization, V.V.P. and A.A.C.; methodology, V.V.P. and A.A.C.; investigation, V.V.P., A.A.C. and D.S.G.; data curation, V.V.P. and A.A.C.; writing—original draft preparation, V.V.P., A.A.C. and D.S.G.; writing—review and editing, V.V.P. and D.S.G.; supervision, V.V.P. All authors have read and agreed to the published version of the manuscript.

Funding: This research received no external funding.

Institutional Review Board Statement: Not applicable.

Informed Consent Statement: Not applicable.

Data Availability Statement: The data presented in this study are available on request from the corresponding author.

Conflicts of Interest: The authors declare no conflict of interest.

References

1. Meng, L.; Duwal, S.; Lane, J.M.D.; Ao, T.; Stoltzfus, B.; Knudson, M.; Park, C.; Chow, P.; Xiao, Y.; Fan, H.; et al. Pressure Induced Assembly and Coalescence of Lead Chalcogenide Nanocrystals. *J. Am. Chem. Soc.* **2021**, *143*, 2688–2693. [CrossRef] [PubMed]
2. Dubey, R.; Rajesh, Y.; More, M. Synthesis and Characterization of SiO_2 Nanoparticles via Sol-gel Method for Industrial Applications. *Mater. Today Proc.* **2015**, *2*, 3575–3579. [CrossRef]
3. Duan, H.; Wang, D.; Li, Y. Green chemistry for nanoparticle synthesis. *Chem. Soc. Rev.* **2015**, *44*, 5778–5792. [CrossRef] [PubMed]
4. Potapov, V.; Fediuk, R.; Gorev, D. Obtaining sols, gels and mesoporous nanopowders of hydrothermal nanosilica. *J. Sol-Gel Sci. Technol.* **2020**, *94*, 681–694. [CrossRef]
5. Potapov, V.; Fediuk, R.; Gorev, D. Hydrothermal SiO_2 Nanopowders: Obtaining Them and Their Characteristics. *Nanomaterials* **2020**, *10*, 624. [CrossRef]
6. Potapov, V.; Fediuk, R.; Gorev, D. Membrane concentration of hydrothermal SiO_2 nanoparticles. *Sep. Purif. Technol.* **2020**, *251*, 117290. [CrossRef]
7. Potapov, V.; Efimenko, Y.; Fediuk, R.; Gorev, D. Effect of hydrothermal nanosilica on the performances of cement concrete. *Constr. Build. Mater.* **2020**, *269*, 121307. [CrossRef]
8. Iler, R.K. Polymerization of polycilicic acid derived from 3.3 ratio sodium silicate. *J. Phys. Chem.* **1953**, *57*, 604–607. [CrossRef]

9. Alexander, G.B. The Reaction of Low Molecular Weight Silicic Acids with Molybdic Acid. *J. Am. Chem. Soc.* **1953**, *75*, 5655–5657. [CrossRef]
10. Alexander, G.B. The Polymerization of Monosilicic Acid. *J. Am. Chem. Soc.* **1954**, *76*, 2094–2096. [CrossRef]
11. Schwarz, R.; Knauff, K.G. Zur Kenntnis der Kieselsäuren. X. Über Alkoxysilane und Oligokieselsäuren. *Z. Für Anorg. Und Allg. Chem.* **1954**, *275*, 176–192. [CrossRef]
12. Bechtold, M.F. Polymerization and Properties of Dilute Aqueous Silicic Acid from Cation Exchange. *J. Phys. Chem.* **1955**, *59*, 532–541. [CrossRef]
13. Goto, K.J. States of silica in aqueous solutions. II. *Chem. Soc. Jap. Pure Chem. Sect.* **1955**, *76*, 1364–1366.
14. Hoebbel, D.; Wieker, W. Über Kondensationsreaktionen der Monokieselsäure. *Z. Für Anorg. Und Allg. Chem.* **1973**, *400*, 148–160. [CrossRef]
15. Hoebbel, D.; Wieker, W. Über die dünnschichtchromatographische Trennung trimethylsilylierter Kieselsäuren. *Z. Anorg. Allgem. Chem.* **1974**, *405*, 163–166. [CrossRef]
16. Hoebbel, D.; Wieker, W.; Hoebbel, D.; Wieker, W. 29Si-NMR-Spektroskopie an Silicatlösungen. IV. Untersuchungen zur Kondensation der Monokieselsäure. *Z. Für Anorg. Und Allg. Chem.* **1977**, *428*, 43–52.
17. Baumann, H. Polymerization and depolymerization de kieselsaure unter verschiedenen begingungen. *Kolloid-Z.* **1959**, *162*, 28–35. [CrossRef]
18. Ginzburg, F.L.; Sheidina, L.D. Radiochemistry. **1973**, *15*, 410. Available online: http://sciencejournals.ru/journal/radkhim/ (accessed on 18 September 2022).
19. Goto, K. Effect of pH on Polymerization of Silicic Acid. *J. Phys. Chem.* **1956**, *60*, 1007–1008. [CrossRef]
20. Okkerse, C. Submicroporous and Macroporous Silica. Ph.D. Thesis, Delftsche Uitgevers Maatschappif N.V., Delft, The Netherlands, 1961.
21. Richardson, E.; Waddams, J.A. Use of the silico-molybdate reaction to investigate the polymerization of low molecular weight silicic acids in dilute solutions. *Res. Corresp.* **1954**, *7*, 43.
22. Tarutani, T. Chromatographic behavior of silicic acid on sephadex columns. *J. Chromatogr.* **1970**, *50*, 523–526. [CrossRef]
23. Makrides, A.K.; Turner, M.; Slaughter, J. Condensation of silica from super-saturated silicic acid solutions. *J. Colloid Interface Sci.* **1980**, *73*, 345–367. [CrossRef]
24. Frolov, Y.G.; Shabanova, N.A.; Popov, V.V. Influence of temperature and pH on polycondensation of silicic acid in an aqueous medium. *Colloid. J.* **1983**, *45*, 179–182.
25. Frolov, Y.G.; Shabanova, N.A.; Popov, V.V. Polycondensation silicic acid in an aqueous medium. Influence of the concentration of silicic acid. *Colloid. J.* **1983**, *45*, 382–386.
26. Rothbaum, H.; Rohde, A. Kinetics of silica polymerization and deposition from dilute solutions between 5 and 180 °C. *J. Colloid Interface Sci.* **1979**, *71*, 533–559. [CrossRef]
27. Coudurier, M.; Baudru, R.; Donnet, J.B. Etude de la polycondensation de l'acide disilique. *Bull. Soc. Chem. Fr.* **1971**, *9*, 3154–3160.
28. Fleming, B.A. Kinetics of reaction between silicic acid and amorphous silica surfaces in NaCl solutions. *J. Colloid Interface Sci.* **1986**, *110*, 40–64. [CrossRef]
29. Weres, O.; Yee, A.; Tsao, L. Kinetics of silica polymerization. *J. Colloid Interface Sci.* **1981**, *84*, 379–402. [CrossRef]
30. Conrad, C.F.; Icopini, G.A.; Yasuhara, H.; Bandstra, J.Z.; Brantley, S.L.; Heaney, P.J. Modeling the kinetics of silica nanocolloid formation and precipitation in geologically relevant aqueous solutions. *Geochim. Et Cosmochim. Acta* **2007**, *71*, 531–542. [CrossRef]
31. Garofalini, S.H.; Martin, G. Molecular Simulations of the Polymerization of Silicic Acid Molecules and Network Formation. *J. Phys. Chem.* **1994**, *98*, 1311–1316. [CrossRef]
32. Rao, N.Z.; Gelb, L.D. Molecular Dynamics Simulations of the Polymerization of Aqueous Silicic Acid and Analysis of the Effects of Concentration on Silica Polymorph Distributions, Growth Mechanisms, and Reaction Kinetics. *J. Phys. Chem. B* **2004**, *108*, 12418–12428. [CrossRef]
33. Greenberg, S.A. Polymerization of silicic acid in alkaline solutions a kinetics study. *J. Polym. Sci.* **1958**, *27*, 523–527. [CrossRef]
34. Potapov, V.V.; Serdan, A.A.; Kashpura, V.N.; Gorbach, V.A.; Tyurina, N.A.; Zubakha, S.V. Polycondensation of orthosilicic acid in hydrothermal solutions at different temperatures, pH values, and ionic strengths. *Glas. Phys. Chem.* **2007**, *33*, 44–49. [CrossRef]
35. Potapov, V.V.; Cerdan, A.A.; Kashutina, I.A. Numerical Simulation of the Polycondensation of Orthosilicic Acid and of the Formation of Silica Particles in Hydrothermal Solutions. *J. Volcanol. Seism.* **2019**, *13*, 216–225. [CrossRef]
36. Crerar, D.A.; Anderson, G.M. Solubility and solvation reactions of quartz in dilute hydrothermal solutions. *Chem. Geol.* **1971**, *8*, 107–122. [CrossRef]
37. Marshall, W.L. Amorphous Silica Solubilities: I. Behaviour in Aqueous Sodium Nitrate Solutions: 25–300 °C, 0–6 Molal. *Geochim. Cosmochim. Acta* **1980**, *44*, 907–913. [CrossRef]
38. Ohsawa, S.; Kawamura, T.; Nakamatsu, N.; Yusa, Y. Geothermal blue water colored by colloidal silica. In Proceedings of the World Geothermal Congress, Kyushu, Tohoku, Japan, 28 May–10 June 2000; pp. 663–668.
39. Crerar, D.A.; Axtmann, E.V.; Axtmann, R.C. Growth and ripening of silica polymers in aqueous solutions. *Geochim. Cosmochim. Acta* **1981**, *45*, 1259–1266. [CrossRef]